Case Studies in Construction Materials 16 (2022) e01008

Contents lists available at ScienceDirect

Case Studies in Construction Materials

journal homepage: www.elsevier.com/locate/cscm

Machine learning-based shear capacity prediction and reliability analysis of shear-critical RC beams strengthened with inorganic composites

Tadesse Gemeda Wakjira [a,b], Usama Ebead [a,*], M. Shahria Alam [b]

[a] Department of Civil and Architectural Engineering, College of Engineering, Qatar University, P.O. Box 2713, Doha, Qatar
[b] Applied Laboratory for Advanced Materials & Structures (ALAMS), School of Engineering, The University of British Columbia, Kelowna, BC, Canada V1V 1V7

ARTICLE INFO

Keywords:
Inorganic composites
Retrofitting
Machine learning
Modeling
Reliability analysis

ABSTRACT

The application of inorganic composites has proven to be an effective strengthening technique for shear-critical reinforced concrete (RC) beams. However, accurate prediction of the shear capacity of RC beams strengthened with inorganic composites has been a challenging problem due to its complex failure mechanism and the interaction between the internal and external shear reinforcements. Besides, the predictive capabilities of the existing models are not satisfactory. Thus, this research proposed machine learning (ML) based models for predicting the shear capacity of RC beams strengthened in shear with inorganic composites, for the first time, considering all important variables. The results of the analyses evidenced that the proposed ML models can be successfully used to predict the shear capacity of shear-critical RC beams strengthened with inorganic composites. Among the ML models examined herein, the extreme gradient boosting (xgBoost) model showed the highest prediction capability. The comparison among the predictions of the proposed xgBoost and existing models evidenced that the efficacy of the xgBoost model is superior to the existing models in terms of accuracy, safety, and economic aspects. Finally, reliability analysis is performed to calibrate the resistance reduction factors in order to attain target reliability indices of 3.5 and 4.0 for the proposed model.

1. Introduction

Recently, advanced composites have been increasingly utilized as efficient systems for the strengthening of deteriorated reinforced concrete (RC) elements. In this context, fiber reinforced polymer (FRP) has gained immense attention owing to its favorable advantages over traditional strengthening systems, such as ease and speed of installation, high strength and stiffness-to-weight ratio, keeping the geometry of the constituent structure, and high corrosion resistance [1]. However, the presence of epoxy resin in the FRP strengthening systems results in some shortcomings including low compatibility with the concrete substrate, poor performance at elevated temperatures, and irreversibility [1,2]. Consequently, inorganic matrix-based composites, usually referred to as fabric reinforced cementitious matrix (FRCM) have been introduced to alleviate some of the problems associated with FRP counterparts [1]. The FRCM system (referred to as FRCM in subsequent occurrences in this paper), provides better concrete compatibility, higher

* Corresponding author.
E-mail address: uebead@qu.edu.qa (U. Ebead).

https://doi.org/10.1016/j.cscm.2022.e01008
Received 17 November 2021; Received in revised form 21 February 2022; Accepted 10 March 2022
Available online 19 March 2022

permeability, relatively low material cost, and superior behavior at high temperatures [1].

FRCM has been effectively applied for the flexural strengthening of RC beams and slabs [3–6], RC column confinement [7–10], and beam-column joints [11]. Similarly, several experimental investigations have been reported in the literature on the shear behavior of RC beams strengthened with FRCM [2,12–29]. Results from these experiments showed the efficacy of FRCM in enhancing the shear behavior of RC beams. The shear strengthening effectiveness of FRCM system varies with different variables such as the internal shear reinforcement ratio [20,26,30], strength of concrete substrate [16], strengthening configuration (continuous versus discontinuous) [17,27,31], wrapping scheme (full wrap, U-wrap, and side bonded) [24,32], and axial rigidity of FRCM composite [20,30,31].

Despite a considerable amount of experimental investigations on FRCM strengthening of RC beams, there are limited analytical studies aimed to understand their structural behavior, particularly those shear strengthened [2,25,27,33–35]. Accurate determination of the shear capacity of the strengthened beams is imperative for achieving a safe and economic design. However, the accuracy of the available shear models and guideline formulae is limited as these equations were mainly developed empirically based on predefined forms of equation. Moreover, the associated experimental datasets have mainly been generated for a limited number of important variables. Besides, these models generally fail to consider the interactions between FRCM and stirrups. This interaction has been reported in previous experiments on shear-critical RC beams strengthened with FRCM [20,26,30,36,37]. It is also known that the shear failure of FRCM strengthened RC beams involves a complicated mechanism due to the FRCM/stirrup interactions [30]; hence, such type of failure has not yet been completely addressed. Thus, it is crucial to develop an accurate and reliable shear model to avoid catastrophic shear failure that occurs without any prior signs of damage.

The use of supervised machine learning (ML) techniques for modeling different civil engineering structures has recently acquired considerable attention owing to its ability to determine the relationship between the input variables and response(s) without prior assumptions of the underlying mathematical and physical models [38] in contrast to most empirical models. It has been successfully applied to solve different problems including damage assessment of bridges [39–42] and buildings [43], prediction of material properties [44–47], and load-carrying capacity and failure mode of RC members [48–58]. A review of the application of different ML techniques in structural engineering is conducted by Salehi and Burgueño [59].

Previously, single ML models were mainly adopted in the literature including artificial neural network [60–63], decision trees [64], and support vector machine [47,65]. Generally, a single learner might not be sufficient; thus, multiple base learners can be combined to generate a strong model. In this context, ensemble learners combine multiple base learners (aka weak learners) to produce a more stable and accurate prediction. In ensemble models, new predictions are obtained by combining predictions from each base learner. Ensemble models can be formed by training base learners in parallel (e.g., random forest) or sequentially (e.g., gradient boosting and extreme gradient boosting). Successful applications of ensemble learners have been reported in the literature (e.g. [48,66–71]). However, the literature lacks the application of ML models for predicting the shear capacity of FRCM-strengthened shear-critical RC beams.

Thus, this study proposed an ML-based model, arguably for the first time, to predict the capacity of RC beams strengthened in shear with the FRCM system. Six different types of ML models are evaluated to propose the best ML model for predicting the shear capacity of the strengthened beams. The proposed ML-based model is compared with the existing models and guidelines. The results of the analyses evidenced that the proposed model is superior to other existing models and guidelines in predicting the shear capacity of the FRCM-shear strengthened beams. Moreover, the reliability analysis is performed, for the first time, to calibrate strength reduction factors to achieve specified target reliability levels for the proposed ML model.

2. Existing models and design guideline

Fig. 1 shows the details of an RC beam strengthened in shear with FRCM applied in U-wrapping scheme. In most of the existing design models [2,25,27,33], the shear capacity of the FRCM-strengthened RC beam is evaluated as a simple superposition of the capacity provided by concrete, stirrups, and FRCM system, as follows:

$$V = V_c + V_S + V_f \tag{1}$$

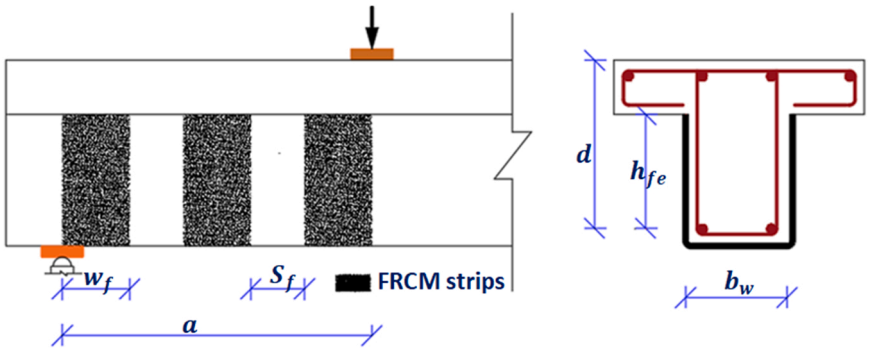

Fig. 1. Details of RC beams strengthened in shear within the shear span with UW FRCM.

where V_c, V_S, and V_f denote concrete, stirrups, and FRCM contributions to shear capacity, respectively.

The existing shear models for RC beams strengthened in shear with FRCM are summarized in Table 1. The first four models [2,25,27,33] generally differ in the evaluation of the FRCM contribution. In two of the models; namely, Triantafillou and Papanicolaou [2] and Escrig et al. [25] models, the shear capacity provided by the FRCM system is determined as a function of the FRCM fiber properties, while ACI 549 [33] and Ombres [27] models are based on the properties of FRCM composite. Model-1 through Model-4 fail to consider the FRCM/stirrups interaction. Moreover, the models do not account for the variation of the shear crack with both applied load and axial tensile strain in the flexural reinforcement bars. As a result, Wakjira and Ebead [34] proposed an analytical procedure based on the modified compression field theory [72], in which the shear capacity of the FRCM-strengthened beams is determined in an iterative procedure considering the effect of FRCM/stirrups interaction and change in the shear crack angle. In another study [35], the same authors used a simplified compression field theory (SCFT) combined with probability and statistical techniques to develop a non-iterative simplified shear design equation for FRCM-strengthened RC beams.

3. Development and normalization of database

It is well understood that the first step in the ML model involves the collection of a relevant experimental database. In this study, a database of 173 FRCM-strengthened RC beams is developed based on an extensive literature review [2,12–20,22–29,31,73–77]. The experimental database covers a wide range of beam geometries, concrete strengths, internal shear and flexural reinforcements, FRCM types, strengthening configurations, wrapping schemes, and mechanical properties of FRCM. Three types of wrapping schemes are used in the database; namely, side bonded (SB) scheme in which the FRCM is bonded to the two sides of the beam, U-wrapped (UW) scheme in which the FRCM is applied to the bottom and two sides of the beam, and full wrapping (FW) schemes. The FRCM composite is applied to the top, bottom, and two sides of the beam in the FW scheme.

Table 1
Existing models for determining the shear capacity of FRCM-strengthened RC beams.

Ref.	Shear capacity models	
Triantafillou and Papanicolaou [2] (Model-1)	$V_f = \rho_f \varepsilon_{eff} E_f b_w h_{fe}$	(2)
	$h_{fe} = 0.9d$ for rectangular beams; $\varepsilon_{eff} = 0.5\varepsilon_{fu}$	
Escrig et al. [25] (Model-2)	$V_f = 2n_f \varepsilon_{eff} E_f t_f h_{fe}(cot\alpha + cot\theta)sin^2\alpha$	(3)
	$\varepsilon_{eff} = k_1 \left(\frac{f_c^{'2/3}}{\rho_f E_f}\right)^{k_2} \varepsilon_{fu} (f_c^{'} \text{ in MPa}, E_f \text{ in GPa})$	(3a)
	θ is assumed to be 45°;	
	$k_1 = 0.02$; $k_2 = 0.55$ for side bonded or U-wrap scheme and	
	$k_1 = 0.035$; $k_2 = 0.650$ for fully wrapped scheme.	
Ombres [27] (Model-3)	$V_f = k_e \varepsilon_{eff} E_{frcm} \rho_f b_w d(cot\alpha + cot\theta)\, sin\alpha$(4)	(4)
	$\varepsilon_{eff} = \frac{f_{fdd}}{E_{frcm}}\left[1 - \frac{1}{3}\frac{l_e sin\alpha}{min(0.9d;\ h_w)}\right]$	(4a)
	$f_{fdd} = \frac{0.24}{\gamma_{fd}\sqrt{\gamma_c}}\sqrt{\frac{E_{frcm} k_b \sqrt{f_{ck} f_{ctm}}}{t_f}}$	
	$f_{ctm} = 0.30 f_{ck}^{2/3}$; $l_e = \left[\frac{E_{frcm} t_f}{2 f_{ctm}}\right]^{0.5}$; $k_b = \left[\frac{2 - w_f/b}{1 + w_f/400}\right]^{0.5}$; $k_e = 0.5$	(4b)
	$b = \begin{cases} s_f; \text{ discontinuous FRCM } \textit{configuration}; \\ 0.9d\sin(\alpha+\theta)/\sin\alpha; \text{ continuous FRCM } \textit{configuration} \end{cases}$	
	θ is assumed to be 45°; $w_f/b \le 0.33$	
	k_e = effectiveness coefficient assumed to be 0.50;	
	l_e = optimal bond length; k_b = geometric coefficient	
ACI 549 [33] (Model-4)	$V_f = n_f A_f \sigma_{eff} d$	(5)
	$\sigma_{eff} = \varepsilon_{eff,FRCM} E_{FRCM}$, $\varepsilon_{eff,FRCM} = \varepsilon_{FRCM,u} \le 0.004$	(5a)
Wakjira and Ebead [34] (Model-5)	$V = \beta\sqrt{f_c^{'}} b_w d + (R_s \rho_{sy} f_{sy} + \rho_f f_f) b d cot\theta$	(6)
	θ is determined using SCFT[72]	
Wakjira and Ebead [35] (Mobdel-6)	$v = 0.855(f_c^{'})^{0.38} \sqrt[4]{\rho_{sx}} + 1.286(\rho_{sy} f_{sy})^{0.84} + 3.608 K_f^{0.97} (\text{in MPa})$	(7)
	$K_f = \rho_f E_f$	(7a)
	$V = v b_w d$	(7b)

where ρ_f is reinforcement ratio of FRCM, h_{fe} is effective depth of FRCM jacket (Fig. 1), d is effective depth of the beam section, h_w is height of the beam web, ε_{eff}, ε_{fu}, and E_f are effective strain, ultimate strain, and the elastic modulus of FRCM fibers, respectively, $f_c^{'}$ is concrete compressive strength, n_f is number of fabric layers, α is inclination of the fiber with respect to the longitudinal axis of the beam, FW, UW, and SB indicate wrapping scheme; particularly, full, U-, and side bonded wrapping, respectively, A_f is total area of FRCM, σ_{eff}, $\varepsilon_{eff,FRCM}$, $\varepsilon_{FRCM,u}$, and E_{FRCM} are design tensile strength, effective strain, ultimate strain, and elastic modulus of the FRCM composite, R_s is FRCM/stirrups interaction factor, β is tensile stress factor of the cracked concrete, and f_f is effective stress in FRCM.

The development of an accurate shear model requires the incorporation of all parameters affecting the shear capacity of FRCM-strengthened beams. Thus, in this research, a comprehensive set of parameters (a total of 17 parameters) are considered, unlike the existing models that were developed based on a limited number of parameters. These parameters are the width of the web (b_w), effective depth of the section (d), shear span-to-effective depth ratio (a/d), concrete compressive strength ($f_c^{'}$), flexural reinforcement ratio (ρ_{sx}), yield strength of reinforcing flexural bars (f_{sx}), reinforcement ratio of stirrups (ρ_{sy}), yield strength of stirrups (f_{sy}), and characteristics of the FRCM system including the fabric type, tensile strength of the fibers (f_{fu}), elastic modulus of the fibers (E_f), effective depth (h_{fe}) (Fig. 1), thickness of FRCM (t_f), number of FRCM strips (N_f) and width of each strip (W_f) (for discontinuous configuration), number of FRCM layers (n_f), and wrapping scheme. The variables W_f, N_f, n_f, and t_f are used in the model in terms of the FRCM reinforcement ratio (ρ_f) as given by:

$$\rho_f = 2\frac{N_f W_f}{a}\frac{n_f t_f}{b_w} \tag{8}$$

where a is the shear span.

Thus, fourteen (14) parameters are used as the final input vectors of the ML model. Five different types of FRCM fabrics are included in the collected experimental database; namely, carbon (C), basalt (B), glass (G), polyparaphenylene benzobisoxazole (PBO), and steel (S). The G, C, PBO, B, and S fabrics are identified with values 1, 2, 3, 4, and 5 in the ML model. Similarly, all the three wrapping schemes; viz., FW, UW, and SB schemes are included in the database and assigned values of 1 for the SB and 2 for the UW/FW schemes.

Table 2 presents a summary of the geometry and internal reinforcement properties of the experimental tests included in the database along with the descriptive statistics of each parameter, while Table 3 provides a summary of the characteristics of the strengthening system. Besides, Fig. 2 illustrates the statistical distribution of the database in terms of the input parameters versus experimental shear capacity (V_{exp}) plots.

4. Overview of ML models

This section presents an overview of the ML models used in this study. Six ML models are evaluated to establish a shear capacity prediction model for RC beams strengthened in shear with FRCM, as discussed below.

Table 2
Geometry and material characteristics of the beams included in the database.

References	Geometry			Concrete	Internal reinforcement			
	b_w (mm)	d (mm)	a/d	$f_c^{'}$ (MPa)	ρ_{sx} (%)	f_{sx} (MPa)	ρ_{sy} (%)	f_{sy} (MPa)
[12]	180	419	2.98	46.2	3.20	555	–	–
[22]	150	159	2.52	20	1.30	578	–	–
[23]	150	307.5	3.25	37.5	2.17	480	–	–
[24]	102	177	2.60	21.6–23.8	2.23	547	–	–
[25]	300	254	2.76	28–28.3	0.79	517.2	–	–
[26]	150	250	3.00	36	5.03	520	0.0–0.50	0.0–294
[27]	150	225	2.78–3.0	29.2–38.3	1.86–2.79	457	0.23–0.32	446
[28]	200	385	2.63	14–15.2	3.26	571	–	–
[29]	150	256	3.91	23.2	3.20	500	–	–
[13]	250	317	3.15	61	3.72	494	0.0–0.75	0.0–365
[14]	102	177	2.6–3.6	20–23.8	2.20	547	–	–
[2]	150	272	2.85	25.3	1.50	575	0.14	275
[15]	120	372	2.69	25.5–34	4.20	500	0.42	500
[16]	152	248	3.00	29.1–42.9	3.04	690	0.27	276
[17]	120	204	3.18	25.6–35.2	2.60	570	–	–
[18]	150	320	2.50	10.1–20.8	1.60	545	–	–
[19]	150	270	2.22	28	1.50	515	–	–
[20]	150	230	3.00	21.3–24.7	6.16	545	0.22–0.34	527
[31]	150	289	1.90	30	1.39	595	–	–
[73]	150	242	3.31	45.95	4.33	526	0.27	526
[74]	200	273	2.20	23.3–28	0.75–1.60	500	–	–
[75]	180	329.5	2.88	34	4.14	588	0.10–0.21	234
[76]	180	334	1.6–3.1	34	2.61	584	–	–
[77]	180	334	2.60	34	2.61	584	–	–
Mean	160	276	2.72	30.5	2.69	543.8	0.09	129.0
STD	41	66	0.46	10.1	1.32	44.3	0.16	203.5
Minimum	102	159	1.60	10.1	0.75	457.2	0	0
25%	150	230	2.50	23.3	1.60	515	0	0
50%	150	272.7	2.69	29.1	2.60	545	0	0
75%	180	320	3.00	35.2	3.72	578	0.21	276
Maximum	300	419	4.90	61	6.16	690	0.75	527

STD: standard deviation.

Table 3
Summary of the strengthening system included in the database.

References	Fabric type	E_f (*GPa*)	f_{fu} (*MPa*)	Wrapping scheme	ρ_f (‰)	h_{fe} (*mm*)
[12]	C	201–262	2950–3800	SB	0.20	377.1
[22]	B	31.9	623	SB	1.20–3.40	143.1
[23]	G, C	75–230	2300–3800	SB, UW	0.49–1.18	276.75
[24]	C	225	3800	SB, FW	1.86–5.59	159.3
[25]	B, G, C, PBO	90–270	2610–5800	FW	0.28–0.35	228.6
[26]	C	230	3800	SB	1.92–3.84	225
[27]	PBO	270	5800	UW	0.30–1.20	202.5
[28]	C	74–225	1400–4800	UW	1.86–3.80	238.5
[29]	G	75	574	FW	1.50–2.20	230.4
[13]	C	230	3800	SB	0.70–1.41	285.3
[14]	C	225	3800–4800	UW	1.22–6.80	159.3
[2]	C	225	3350	FW	0.60–1.30	244.8
[15]	G	75	574	UW	1.80–5.50	252
[16]	PBO	127	1664	UW	0.61–2.42	223.2
[17]	G	74	1102	SB, UW	0.20–1.20	183.6
[18]	C	225	3375	UW	0.60–2.60	220
[19]	C	240	4300	SB, UW	0.40–2.90	243
[20]	C, S	190–240	3800	UW	0.63–3.60	207
[31]	C, G, PBO	80–270	2600–5800	SB	0.40–0.63	260.1
[73]	PBO	270	5800	UW	0.34	300
[74]	S	190	2800	UW, FW	0.84–2.54	245.5
[75]	S	190	3000	SB, UW	1.87–3.76	229.5
[76]	S	190	3000	UW	1.87–3.76	300.6
[77]	S	190	3000	SB, UW	1.22–3.76	300.6
Mean	–	192.4	3393	–	1.69	249.4
STD	–	71.1	1496	–	1.42	59.8
Minimum	–	31.9	574	–	0.20	143.1
25%	–	190.0	2800	–	0.60	207.0
50%	–	225.0	3800	–	1.30	245.5
75%	–	240.0	4300	–	2.46	288.0
Maximum	–	270.0	5800	–	6.80	377.1

STD: standard deviation; C: carbon; G: glass; PBO: polyparaphenylene benzobisoxazole, B: basalt; S: Steel; SB: side bonded; UW: U-wrapping; FW: full wrapping

4.1. Support vector machine

Support vector machine (SVM) is one of the supervised ML techniques with associated algorithms primarily applied for classification problems using structural risk minimization principle [78]. It can also be used to efficiently perform non-linear regression by indirectly mapping the original input vectors into a very high-dimensional feature space, using kernel functions [78]. The class of SVM used for regression problems is known as support vector regression (SVR). Given a set of training sample $\{(x_1, y_1), (x_2, y_2), \ldots, (x_n, y_n)\}$, support vector regression estimate the regression function $f(x)$ in Eq. (9) with a maximum deviation of ε from the observed response for the complete training dataset.

$$f(x) = \sum_{i=1}^{n} (\alpha_i - \alpha_i^*) K(x_i, x) + b \tag{9}$$

$$0 \le \alpha_i, \quad \alpha_i^* \le C \tag{9a}$$

Where $K(x_i, x)$ is a kernel function, b is the bias, α_i and α_i^* are the Lagrange multipliers, and C is a regularization parameter. The widely used kernels are [79,80]:

- Linear kernel: $k(X_i, X_j) = \langle X_i, X_j \rangle$.
- Polynomial kernel: $k(X_i, X_j) = (\gamma \langle X_i, X_j \rangle + r)^d$, $\gamma > 0$ and d as a polynomial degree.
- Hyperbolic tangent (sigmoid) kernel: $k(X_i, X_j) = \tanh(\gamma \langle X_i, X_j \rangle + r)$, $\gamma > 0$.
- Radial basis function (RBF) kernel: $k(X_i, X_j) = e^{-\frac{1}{2\sigma^2} \|X_i - X_j\|^2}$, where σ is the width of the kernel.

In this study, all the above four kernel functions are considered. The other two hyperparameters that greatly affect the SVM predictive capacity are the regularization parameter C and ε-insensitive zone [81]. These hyperparameters are also optimized in this study.

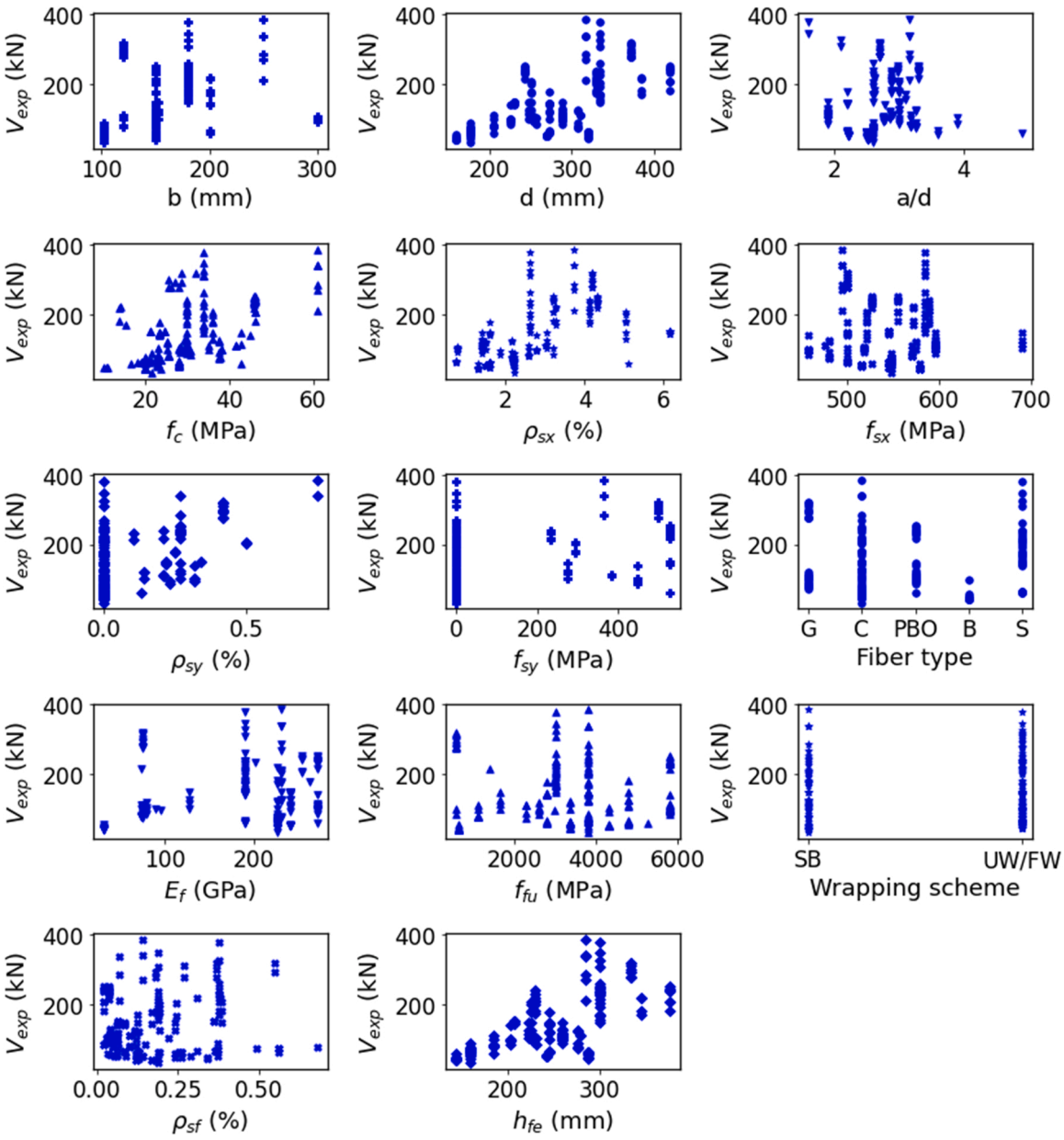

Fig. 2. Correlation between the input parameters and the shear capacity.

4.2. Decision trees

Decision tree aka classification and regression tree or CART for short is a non-parametric supervised ML algorithm that resembles a flowchart-like structure. The CART algorithm predicts the response following the decision from the root node to the leaf, in which each internal node or decision node denotes the test, while each leaf or terminal node represents the outcome of the test.

It can be used to solve both classification and regression problems in the form of a tree structure [64]. In regression, given n observations of training dataset $\{(x_1, y_1), (x_2, y_2), \ldots, (x_n, y_n)\}$, decision tree iteratively splits the training data into a set of terminal nodes. The algorithm then fits a regression tree in each node using the feature, which produced the highest information gain at each node [64]. The main hyperparameters of the CART; namely, the maximum depth of the tree, minimum number of samples required to split the internal node, minimum number of samples at the leaf node, and maximum number of input features at each node are optimized to determine the best model.

The decision tree model is easy to interpret and visualize. However, a single tree may not be adequate to effectively learn the model. Furthermore, decision tree suffers from the problem of generalization and high variance and bias. The ensemble of CARTs can be used

to overcome these problems.

4.3. Random forest

Random forest is an ensemble model that constructs several decision trees in parallel as a committee to generate independent outputs, and finally computes their mean to generate the final output in order to ultimately increase the prediction accuracy of the underlying algorithms [82]. In this sense, random forest follows a two-step process: (a) construct T number of decision trees (estimators) and (b) compute the arithmetic mean of the predictions across the estimators to generate the final prediction in the case of regression and a majority vote in the case of classification problems. In growing the trees, random forest regression (RFR) uses randomly selected input data with replacement (bootstrap samples) from the training dataset. Moreover, an optimal number of input features is chosen at each node. Random forest uses different hyperparameters including the number of estimators, which is the maximum number of trees that the algorithm uses to make the prediction, maximum number of randomly chosen features to be included at each node split, minimum number of samples at the leaf node, and maximum depth that a tree can grow.

4.4. Extremely randomized trees

Extremely randomized trees (ERT) algorithm is another type of tree ensemble learners that can be applied to both classification and regression problems [83]. Its main difference with the random forest is that it uses the complete training dataset to grow the trees, unlike random forest that uses bootstrap samples. Besides, ERT adds randomization in selecting the split points of each node [83]. Similar hyperparameters are used for the extremely randomized trees as that of random forest.

4.5. Gradient tree boosting

Gradient tree boosting [84] is a class of boosting ensembles, which combines weak learners, particularly decision trees in a sequential form to form a powerful and accurate predictive model. Each decision tree in the sequence learns and improves on the previous one essentially by focusing on the observations with the largest error or residuals in the previous trees. Given n training examples, $X = \{(x_i, y_i)\}_{i=1}^{n}$, in which $x_i \subseteq \mathbb{R}^m$ are feature vector with m input features and $y_i \epsilon \mathbb{R}$ are the response variable, gradient tree boosting regression (GTBR) finds the predictions ($\widehat{y_i}$) as the weighted sum of base learners. Mathematically, the GBTR can be written as:

$$\widehat{y_i} = F_T(x_i) = \sum_{t=1}^{T} f_t(x_i) \tag{10}$$

where T is the total number of estimators (trees) and f_t is the set of all possible decision trees.

The algorithm for the GBTR can be summarized as follows [84]:

1) Initialize the function with a constant.

$$F_0(x) = arg \underset{\rho}{min} \sum_{i=1}^{n} L(y_i, \quad \rho) \tag{11}$$

where L is the loss function.

2) From $t = 1$ to T, repeat the following:

a) Compute the negative gradient of the loss function, given by:

$$g_{it} = -\frac{\partial L[y_i, F_{t-1}(x_i)]}{\partial F_{t-1}(x_i)}, \quad i = 1, \quad 2, \quad \ldots, \quad n \tag{12}$$

a) Fit a new decision tree (f_t) using the training set $\{(x_i, g_{it})\}_{i=1}^{n}$.
b) Compute the multiplier ρ_t, given by:

$$\rho_t = arg \underset{\rho}{min} \sum_{i=1}^{n} L(y_i, F_{t-1}(x_i) + \rho f_t(x_i)) \tag{13}$$

a) Update the ensemble model:

$$F_t(x) = F_{t-1}(x) + v\rho_t f_t(x) \tag{14}$$

where v is the learning rate.

3) Output $F_T(x)$.

The gradient boosting hyperparameters are tuned to produce accurate predictions.

4.6. Extreme gradient boosting

Extreme gradient boosting (xgBoost), proposed by Chen and Guestrin [85], is an enhanced form of gradient boosting. Extreme gradient boosting introduces a regularization parameter (Ω) to prevent model complexity, and thus, reduce overfitting [85]. Hence, the objective function to be optimized in xgBoost consists of two parts in which the second term Ω penalizes the complexity of the model and avoids overfitting, as given below [85].

$$Obj = \sum_{i=1}^{n} L(\widehat{y}_i, y_i) + \sum_{t=1}^{T} \Omega(f_t) \tag{15}$$

$$\Omega(f_t) = \gamma T + \frac{1}{2}\lambda\|\omega\|^2 \tag{16}$$

Where γ is the complexity of each leaf, λ is the penalty parameter, and $\|\omega\|$ is the vector score on the leaves.

5. Hyperparameter optimization

Following the normalization of the database and identification of the input features and response variable, the database is randomly divided into the train and test datasets including 70% and 30% of the complete dataset, respectively. The ML models are then trained using the training set, while the test dataset is used to finally appraise their performance. Several combinations of the hyperparameters are examined to optimize each model using grid search in conjunction with K-fold cross-validation. In the K-fold cross-validation approach, the data is randomly partitioned into 10 parts of equal sizes, and then the $K-1$ folds are used to train the model, while the remaining one-fold is used to validate the model (K = 10 is adopted in this study). Thus, each group, in turn, serves as a validation set and the cross-validation is repeated K times. The performance of the model is then determined as the average of the results from the K data folds. Four statistical performance indices; namely, mean absolute percentage error (MAPE), mean absolute error (MAE), root mean squared error (RMSE), and coefficient of determination (R^2) are used in this study, as given by Eqs. (17a)–(17d), respectively.

$$MAPE = \frac{1}{n}\sum_{i=1}^{n}\left|\frac{y_i - \widehat{y}_i}{y_i}\right| \tag{17a}$$

$$MAE = \frac{1}{N}\sum_{i=1}^{N}|y_i - \widehat{y}_i| \tag{17b}$$

$$RMSE = \sqrt{\frac{1}{n}\sum_{i=1}^{n}(y_i - \widehat{y}_i)^2} \tag{17c}$$

$$R^2 = 1 - \frac{\sum_{i=1}^{n}(y_i - \widehat{y}_i)^2}{\sum_{i=1}^{n}(y_i - \overline{y})^2} \tag{17d}$$

Where y is the observed value, $\widehat{y}$ is the predicted value, and $\overline{y}$ is the arithmetic mean of y values.

Table 4
Optimized hyperparameters.

Models	Parameters
SVR	Kernel = RBF, C = 50, ε = 0.00001, gamma = 'auto'
CART	Maximum depth = 7, maximum features = 8, minimum sample leaf = 1, minimum sample split = 3
RFR	Number of estimators = 6, maximum features = 6, maximum depth = 10, minimum sample leaf = 1, minimum sample split = 3
ERT	Number of estimators = 12, maximum features = 13, maximum depth = 8, minimum sample leaf = 1, minimum sample split = 2
GTBR	Number of estimators = 138, maximum features = 8, learning rate = 0.15, maximum depth = 5, subsample = 0.3, minimum sample split = 2, minimum sample leaf = 1
xgBoost	Number of estimators = 440, learning rate = 0.5, subsample = 0.4, maximum depth = 8, reg lambda = 1, reg alpha = 0, γ = 0, colsample by node = 1.0, colsample by level = 0.9, colsample by tree = 1

6. Results and discussion

The ML models are trained using the optimized hyperparameters presented in Table 4. The performance of ML models is presented in Table 5 in terms of the MAPE, MAE, RMSE, and R^2. In addition, Fig. 3**a–f** compare the predicted (V_{pred}) and experimental (V_{exp}) shear capacities based on the proposed ML models in which the solid line shows the perfect match between V_{exp} and V_{pred}, while the hidden lines denote the 20% overestimation or underestimation of the shear capacity. As can be seen in these figures, the predictions provided by all models are in good agreement with the corresponding experimental values ($R^2 \geq 0.943$ for all models). It can also be observed from the same figures that the xgBoost model produced the best prediction for the shear capacity compared to all other models. A strong correlation exists between the experimental and predicted shear capacities based on the xgBoost model as evidenced by the value of R^2 of 0.995 and 0.984 for the training and test datasets, respectively, as can be seen in Fig. 3**f** and Table 5. The GTBR model was the second best model in predicting the shear capacity of the strengthened beams, as shown in Fig. 3**e** and Table 5.

Moreover, performance evaluation of the ML models showed a very small difference between the experimental shear capacities and the corresponding predicted values using the xgBoost model in the training and test phases as indicated by the RMSE of 5.94 kN and 10.96 kN, respectively. For the SVR, CART, RFR, ERT, and GTBR models, these values were 14.55 kN, 12.23 kN, 12.21 kN, 7.03 kN, and 6.78 kN, respectively, for the training dataset and 19.29 kN, 20.98 kN, 19.48 kN, 16.61 kN, and 13.55 kN, respectively, for the test dataset (Table 5). Thus, the xgBoost model showed the highest predictive capability with the highest R^2 and least MAE, MAPE, and RMSE followed by the GTBR model (Table 5). The superior predictive performance of xgBoost, as an improved version of gradient tree boosting, is associated with the enhanced aspects of the loss function and loss optimization. On the contrary, the CART model showed the least predictive performance on the test dataset with the lowest R^2 ($R^2 = 0.943$) and highest RMSE (20.98 kN), as shown in Fig. 3**a–f** and Table 5.

The prediction performance of the proposed xgBoost model is compared with that of the existing models and design guideline formulae discussed in Section 3. As discussed earlier, Ombres [27] and ACI 549.4R [33] models are based on the properties of the FRCM composite, while Triantafillou and Papanicolaou [2], Escrig et al. [25], and Wakjira and Ebead [34,35] models are based on the fiber properties. Out of the total number of beams included in the database, E_{FRCM} is not reported for 78 beams. As a result, the Ombres [27] and ACI 549.4R [33] models are validated against 95 beams only. Moreover, Wakjira and Ebead [34,35] models are proposed for FRCM-strengthened RC beams with $a/d > 2.5$, thus they are evaluated against 128 beams out of 173 beams. Fig. 4**a–f** show the scatter plots of the experimental versus predicted shear capacities based on the existing models. As can be observed in these figures, Model-1 overpredicted the shear capacity for large number of beams, while the shear capacity for most of the beams are underestimated by Model-2, -3, and -4, as shown in Fig. 4**a–d**. However, the predictions provided by Model-5 and Model-6 are scattered around the equity line that shows the perfect match between the predicted and experimental shear capacities, as shown in Figs. 4**e** and 4**f**. As shown in Fig. 4**a–f,** Model-5, which is based on the modified compression field theory provided the best predictions among the existing models followed by Model-6.

Fig. 5 compares the experimental shear capacity and the corresponding predicted values based on the existing and proposed xgBoost models. As can be observed in this figure, the predictions provided by the proposed model lies within ± 20% error margin for all beams except two, while most of the predictions are highly overestimated or underestimated for the existing models. Besides, the statistical performance indices for the existing and proposed xgBoost models are listed in Table 6 and further illustrated in Fig. 6 in terms of the MAE and RMSE.

The proposed xgBoost model substantially reduced the RSME by 91%, 90%, 92%, 92%, 79%, and 85% compared to Model-1, -2, -3, -4, - 5, and -6, respectively, as shown in Fig. 6 and Table 6. Similarly, the proposed model provided a significantly lower MAE compared to others, as shown in Fig. 6 and Table 6. The mean of the V_{pred}/V_{exp} ratio is 0.99 for the proposed xgBoost model compared with mean values of 1.28, 0.66, 0.53, 0.49, 0.94, and 0.9 for Model-1 through Model-6, respectively, as listed in Table 6. The predictions provided by the proposed xgBoost model was less scattered as evidenced by the standard deviation (STD) for the V_{pred}/V_{exp} ratio value of 0.06 compared to STD values of 0.81, 0.26, 0.25, 0.21, 0.22, and 0.28 for Model-1, -2, -3, -4, -5, and -6, respectively, as listed in Table 6.

The prediction capability of the proposed xgBoost model and existing models was also evaluated in terms of the Modified Demerits Points Classification (MDPC) method [86], in which the penalty assigned to each value of the V_{pred}/V_{exp} ratio is used to evaluate the model's accuracy, safety, and economic aspects as per Table 7. Fig. 7**a–g** compare the prediction capability of the proposed and existing models based on the MDPC method in which 'AS', 'C', 'EC', 'D', and 'ED', donate the appropriate safety, conservative, extra conservative, dangerous, and extra dangerous regions, respectively. As can be seen in these figures, the predictions provided by

Table 5
Performance indices for the proposed models.

Models	Training dataset				Test dataset			
	MAPE (%)	MAE (kN)	RMSE (kN)	R^2	MAPE (%)	MAE (kN)	RMSE (kN)	R^2
SVR	6.69	7.97	14.55	0.968	10.01	13.76	19.29	0.952
CART	4.58	6.86	12.23	0.978	9.36	14.56	20.98	0.943
RFR	7.09	8.60	12.21	0.978	7.96	12.82	19.48	0.951
ERT	3.83	4.35	7.03	0.993	7.37	11.44	16.61	0.964
GTBR	3.50	4.30	6.78	0.993	8.48	10.50	13.55	0.976
xgBoost	1.84	2.62	5.94	0.995	6.16	8.23	10.96	0.984

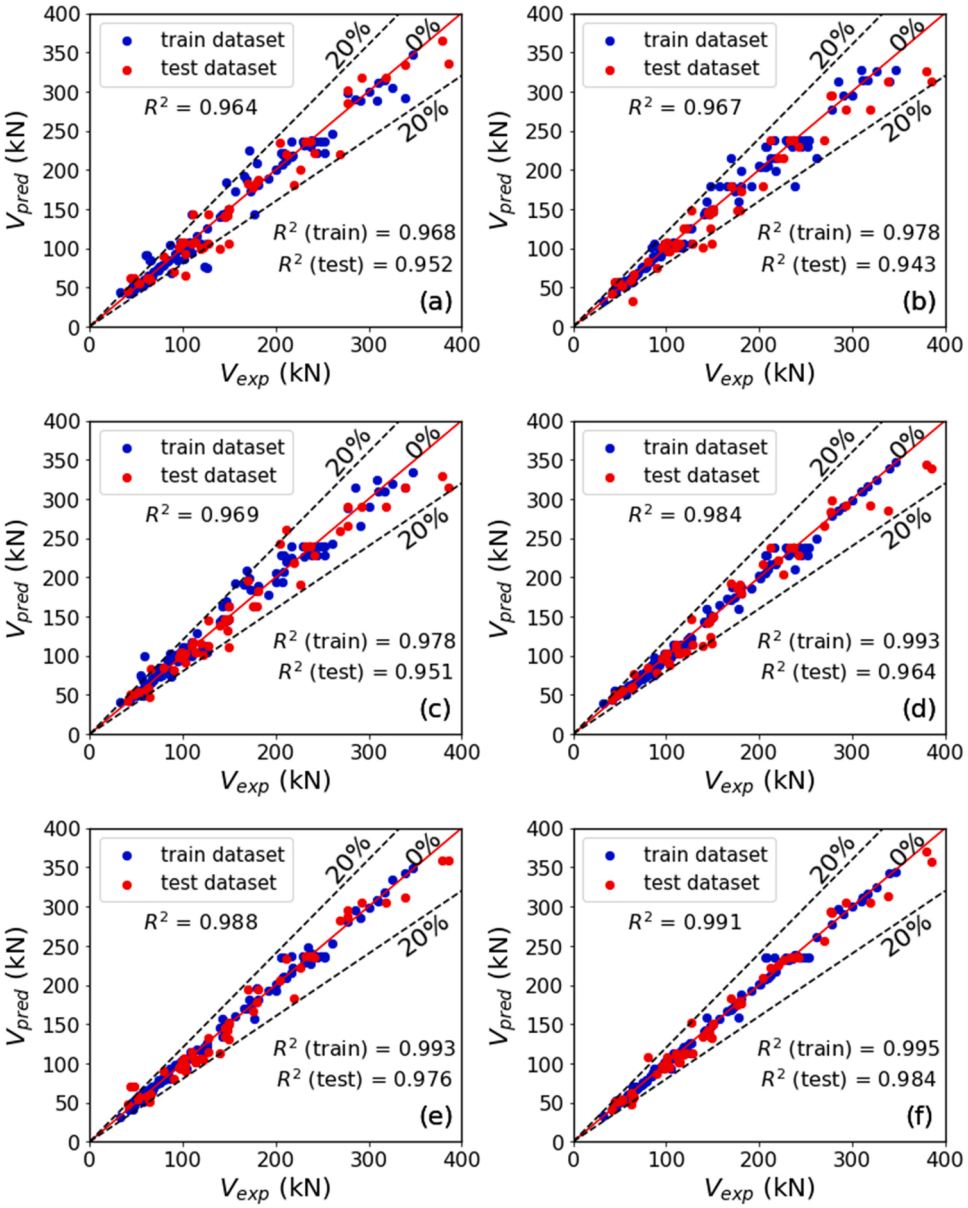

Fig. 3. Comparison of experimental and predicted shear capacities of the strengthened beams based on (a) SVR, (b) CART, (c) random forest, (d) extremely randomized trees, (e) gradient tree boosting, and (f) xgBoost.

Model-1 [2] are most scattered and biased with the least predictive capacity, while the predictions of Model-4 [33] mainly lie in the conservative and extra conservative regions. Among the existing models, Model-5 [34], which is based on the modified compression field theory provided the best predictions followed by Model-6, as can be seen in Fig. 7**a–g**. Table 8 presents the number of beams in each range and the total penalty as per the MDPC method [86] for all models. As can be seen in Fig. 7**a–g** and Table 8**,** the predictions for 98% of the beams, based on the proposed xgBoost model lie in the appropriate safety region compared to only 22%, 18%, 16%, 3%, 51%, and 34% of the beams for Model-1, -2, -3, -4, -5, and -6, respectively. Thus, the proposed xgBoost model exhibited superior predictions with a total penalty of 12 compared to the total penalty of 559, 220, 125, and 190 for Model-1, -2, -5, and -6, respectively, as listed in Table 8. Model-3 and Model-4 are evaluated against 95 beams only and are associated with a total penalty of 144 and 157, respectively, as listed in Table 8. This observation evidenced that the proposed xgBoost model is capable to yield accurate and safe predictions with superior prediction capability compared to the existing models. Generally, the prediction of the proposed model is in an appropriate safety region for all ranges of the input variables, as can be observed in Fig. 8 that shows the input factors versus the predicted-to-experimental shear capacities ratio plots. Compared to RC beams without stirrups, the predictions for RC beams internally reinforced with stirrups are more accurate (Figs. 8**g and** 8**h**). Moreover, the proposed model showed a better prediction accuracy for

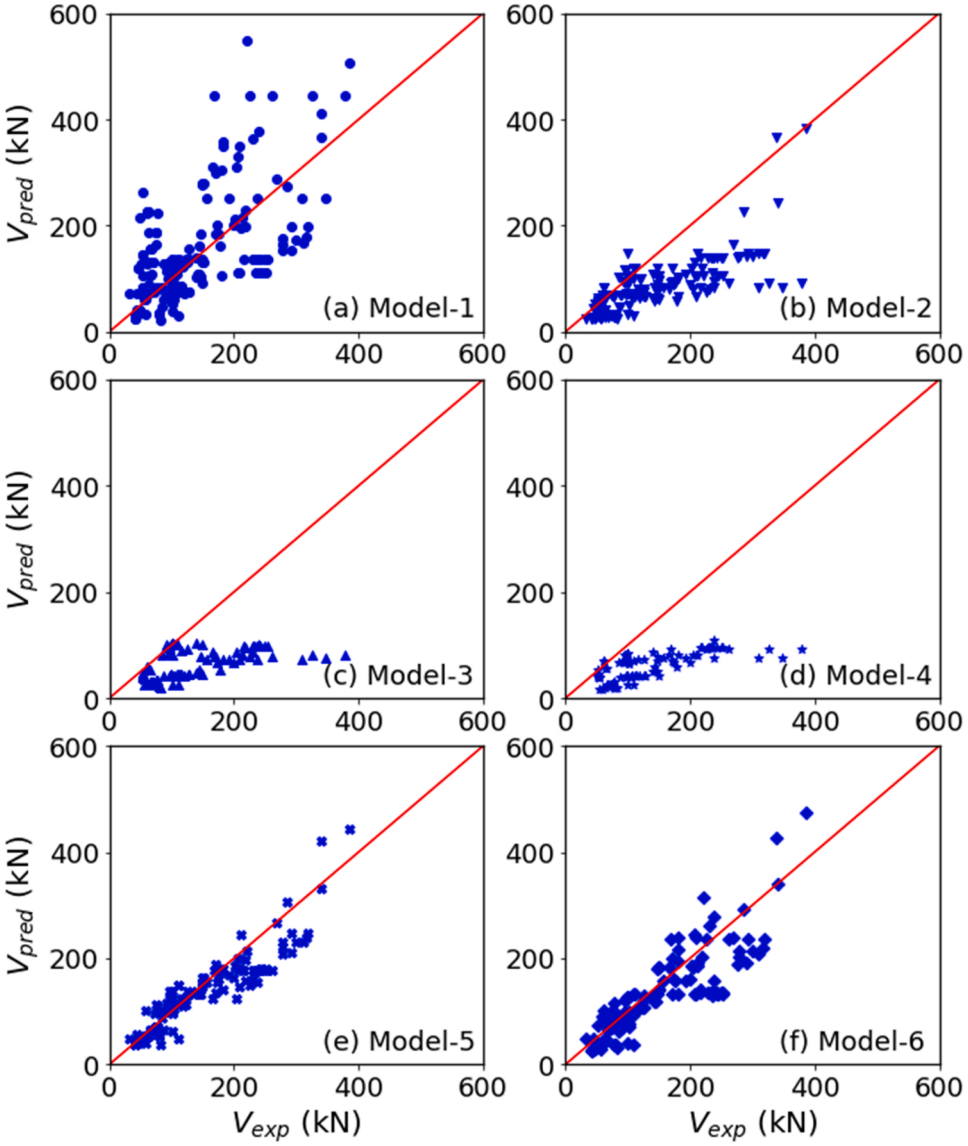

Fig. 4. Predictions of the shear capacity based on the existing models.

RC beams strengthened with side bonded scheme compared to U-wrap or full wrap scheme, as shown in Fig. 8**l**.

7. Reliability evaluation

Reliability analysis is used to estimate the level of safety of a system in terms of its failure probability. Accordingly, structural reliability analysis measures the performance of structures. In this study, the structural reliability analysis is performed for the proposed xgBoost model to calibrate the resistance (strength) reduction factors to achieve specified target reliability indices.

The reliability index (β) can be given by Eq. (18), while Eq. (19) defines the safety margin (g) in terms of the resistance (R) and load effect (Q):

$$\beta = \varphi^{-1}(1 - P_F) \tag{18}$$

$$g = R - Q \tag{19}$$

where P_F is the probability of failure and φ^{-1} is the inverse of standard normal cumulative distribution.

Thus, the probability of failure is the probability that a particular combination of R and Q will result in a failure state which corresponds to a negative value of g. The ultimate limit state load cases as per ACI 318 [87] is used in this study considering only dead

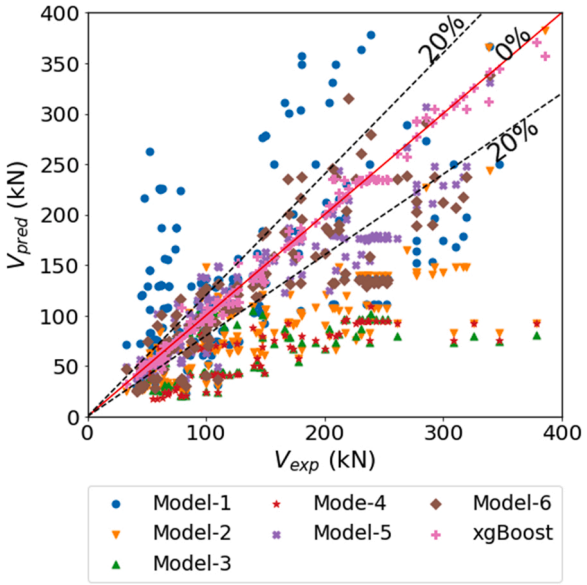

Fig. 5. Comparisons of shear capacity predictions based on the existing and proposed xgBoost models with ± 20% error bounds.

Table 6
Performance of different shear models.

Model	Model ID	Sample size	RMSE (kN)	MAE (kN)	Mean of V_{pred}/V_{exp}	STD of V_{pred}/V_{exp}
Triantafillou and Papanicolaou [2]	Model-1	173	87.02	65.30	1.28	0.81
Escrig et al. [25]	Model-2	173	81.60	60.66	0.66	0.26
Ombres [27]	Model-3	95	97.17	73.86	0.53	0.25
ACI 549.4R [33]	Model-4	95	97.21	77.83	0.49	0.21
Wakjira and Ebead [34]	Model-5	128	37.84	27.97	0.94	0.22
Wakjira and Ebead [35]	Model-6	128	50.29	37.60	0.90	0.28
xgBoost	–	173	7.80	4.30	0.99	0.06

STD: standard deviation.

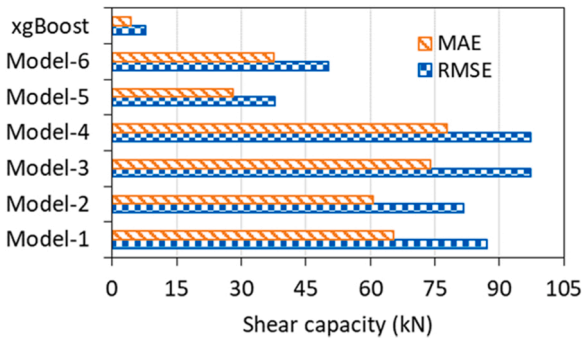

Fig. 6. Comparison of the predictions of the shear models in terms of the RMSE and MAE.

Table 7
Modified Demerits Points Classification criteria [86].

V_{pred}/V_{exp}	Classification	Penalty
> 2	Extra dangerous	10
[1.176–2]	Dangerous	5
[0.869–1.176]	Appropriate safety	0
[0.5–0.869]	Conservative	1
≤ 0.5	Extra conservative	2

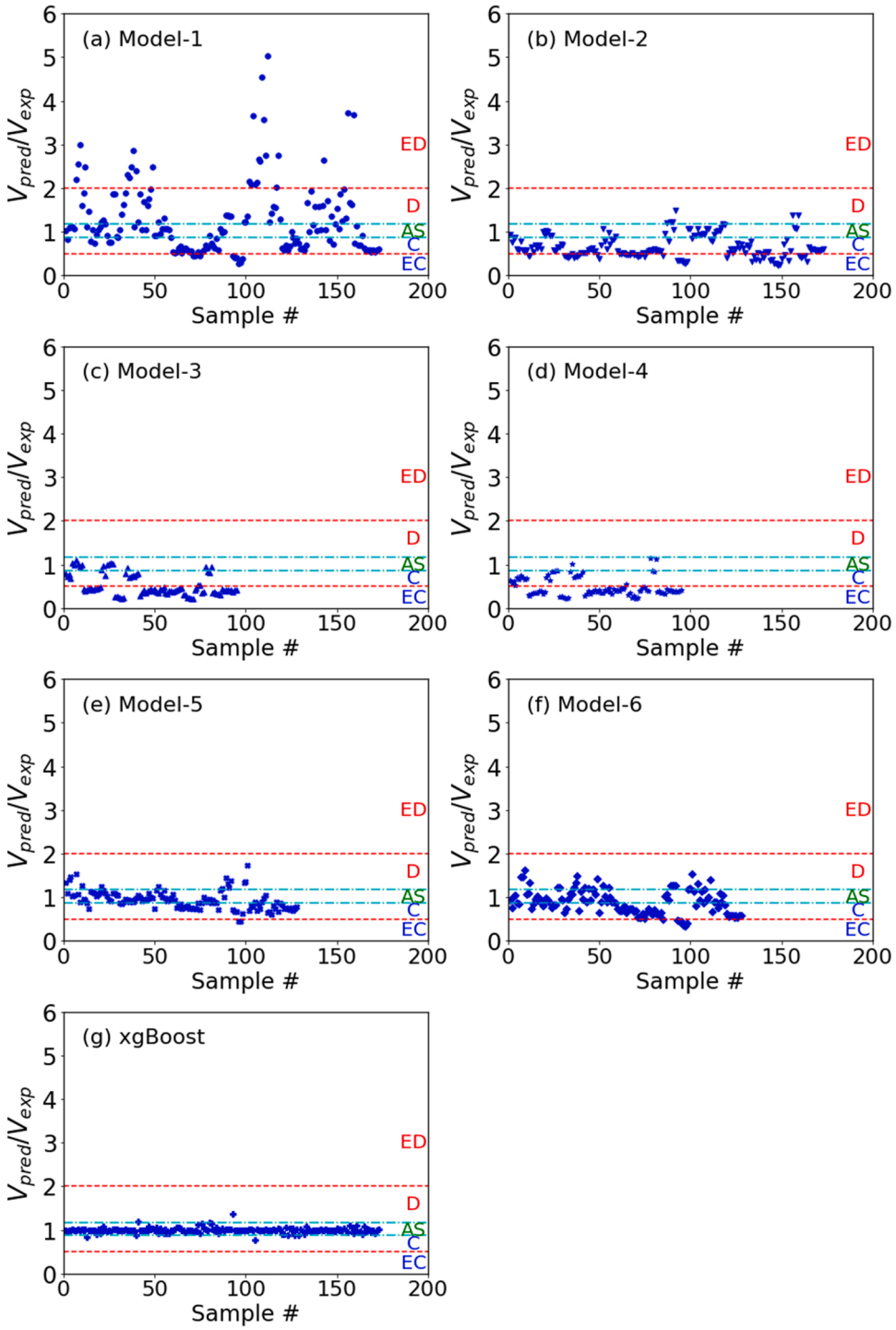

Fig. 7. Prediction capability of the proposed and existing models based on the MDPC method [86].

load (*DL*) and live load (*LL*):

$$\phi R_n \geq 1.4DL \tag{20a}$$

$$\phi R_n \geq 1.2DL + 1.6LL \tag{20b}$$

The following steps are followed in this study to determine the reliability index:

Table 8
Predictive performance of the models based on the Modified Demerits Points Classification [86].

Shear model	Sample size	V_{pred}/V_{exp}	> 2	[1.176–2]	[0.869–1.176]	[0.5–0.869]	≤ 0.5	Total penalty
		Criteria	Extra dangerous	Dangerous	Appropriate safety	Conservative	Extra conservative	
		Penalty	10	5	0	1	2	
Triantafillou and Papanicolaou [2]	173	N	26	45	38	54	10	559
		Penalty	260	225	–	54	20	
Escrig et al.[25]	173	N	–	7	32	83	51	220
		Penalty	–	35	–	83	102	
Ombres [27]	95	N	–	–	15	16	64	144
		Penalty	–	–	–	16	128	
ACI 549.4R [33]	95	N	–	–	3	27	65	157
		Penalty	–	–	–	27	130	
Wakjira and Ebead [34]	128	N	–	15	65	46	2	125
		Penalty	–	75	–	46	4	
Wakjira and Ebead [35]	128	N	–	25	44	53	6	190
		Penalty	–	125	–	53	12	
xgBoost	173	N	–	2	169	2	–	12
		Penalty	–	10	–	2	–	

N: number of samples in the specified range.

- Load distribution: both dead load and live load are assumed to follow a normal distribution [88]. According to Szerszen and Nowak [88], the bias factor for dead load is taken as 1.05 with a coefficient of variation (COV) of 10% for cast-in-place concrete, whereas the bias and COV for a 50 year live load are taken as 1.0% and 18%, respectively. To determine the nominal live load, dead load to total load ratios ($\alpha = DL/(DL + LL)$) of 0–1.0 at 0.1 intervals are considered in this study. A total of 250 million simulations was generated using Monte Carlo simulation for each α. The actual mean is determined as the product of the nominal mean and bias.
- Resistance distribution: the experimental data is used to determine the bias factor and COV of the resistance distribution, while the nominal resistance distribution is determined based on the governing load combination in Eqs. (20a) and (20b).
- The reliability index is then determined in terms of the failure probability in Eq. (18) where P_F is determined based on the ultimate limit state in Eq. (19), where Q is the sum of dead load and live load.

The consequences of failure determines the choice of the target reliability index [89]. According to [89], a value between 3.5 and 4.0 is taken as β_T for brittle/sudden failure. Thus, two levels of target reliability ($\beta_T = 3.5$ and $\beta_T = 4.0$) are considered in this study in order to represent the range of target reliability indices in design manuals for shear failure. The resistance reduction factor is calibrated using the least square method:

$$H = \frac{1}{n}\sum_{i=1}^{n}(\beta_i - \beta_T)^2 \tag{21}$$

where H is the least square mean, β_i is the reliability at a particular ϕ, and β_T is the target reliability, as defined earlier.

Several values of resistance (strength) reduction factor (ϕ) ranging from 0.80 to 0.95 at 0.01 intervals were considered. Similarly, the load ratio ranged between 0.0 and 1.0 at 0.1 intervals. The results of the reliability analysis for the proposed xgBoost model are illustrated in Figs. 9**a** and 9**b** in terms of reliability indices versus resistance reduction factor and load ratio, respectively. As can be seen in these figures, the reliability index varies with the load ratio and ϕ. Most of the reliability indices are greater or equal to 3.0, as shown in Figs. 9**a** and 9**b**. When the live load (LL) is zero, there is a sudden increase in the reliability index as the load factor for LL is higher than that for DL, Eq. (20b). A similar trend can be observed in previous study [88].

Moreover, Fig. 10 illustrates the H_ϕ versus ϕ responses for target reliability indices of 3.5 and 4.0. As can be observed in this figure, H_ϕ initially decreased with an increase in ϕ and subsequently increased with an increase in ϕ. The minimum H_ϕ corresponds to resistance reduction factors of 0.91 and 0.87 for target reliability levels of 3.5 and 4.0, respectively, as shown in Fig. 10. Thus, the calibrated resistance reduction factor is 0.91 to achieve a target reliability index of 3.5, while a reduction factor of 0.87 is selected to yield $\beta_T = 4.0$ for the developed xgBoost model. A lower strength reduction factor of 0.75 is used in the ACI 318 [87] for the shear failure of pristine RC beams compared to $\phi = 0.91$ for xgBoost model proposed in this study for FRCM-strengthened RC beams to achieve the same target reliability level of 3.5. A design example is presented in the following section using the calibrated resistance reduction factor ($\phi = 0.91$) for $\beta_T = 3.5$.

8. Design example

Consider a simply supported shear deficient rectangular RC beam of dimensions 180 × 400 mm ($b \times h$) and a clear span of 1000 mm subjected to two factored point loads of 200 kN on each clear span. Fig. 11 shows the cross-sectional dimensions and reinforcement details of the beam in the shear span. Assuming the following material properties and internal reinforcement, the FRCM strengthening amount needs to be designed.

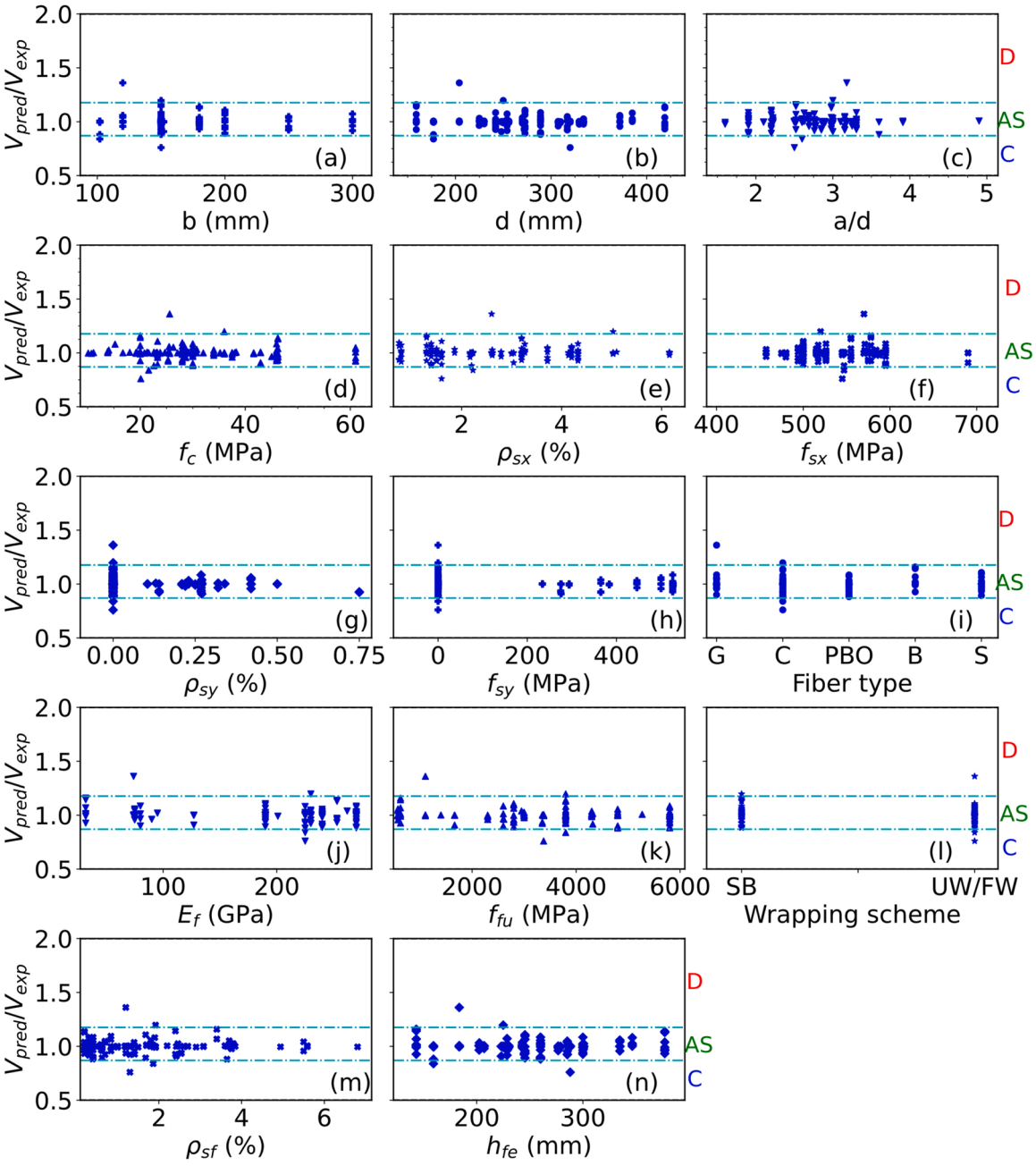

Fig. 8. Input factors versus V_{pred}/V_{exp} ratio plots.

Material properties and internal reinforcement details:

- Concrete: $f_c^{'} = 30$MPa,
- Yield strength of longitudinal bars: $f_{sx} = 550$MPa,
- Yield strength of transverse bars: $f_{sy} = 350$MPa,
- Flexural reinforcement: 6 bars with 20 mm diameter arranged in two layers (Fig. 11),
- Internal transverse reinforcement: 8 mm stirrups spaced at $d/2 = 165$mm (Fig. 11), and
- FRCM properties: uni-directional steel FRCM fabrics with elastic modulus and tensile strength of 190 GPa and 3000 MPa, respectively [90].

The factored load (V_Q) at the supports is 200 kN. The shear capacity of the unstrengthened beam is 169 kN using the SCFT. The

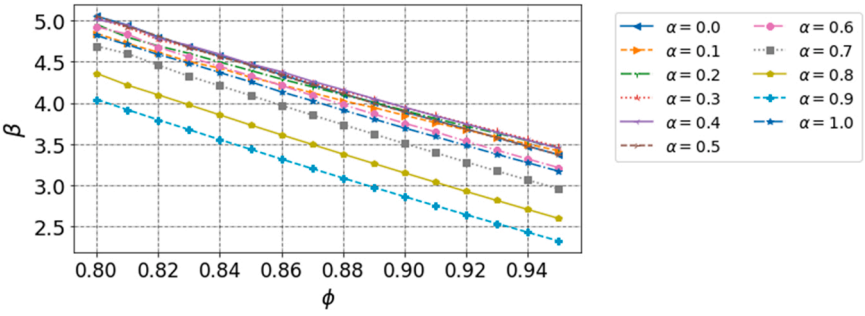

(a) resistance reduction factor (ϕ) versus reliability index (β)

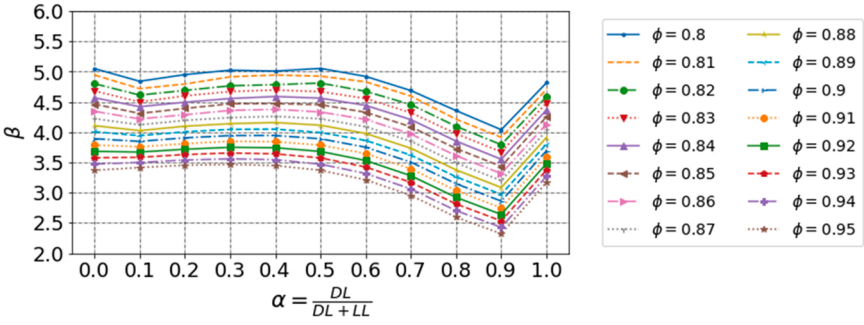

(b) load ratio (α) versus reliability index (β)

Fig. 9. Reliability index for the proposed xgBoost model.

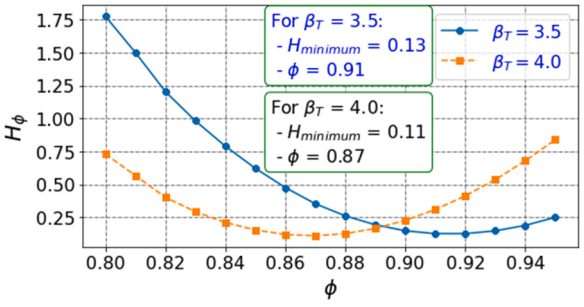

Fig. 10. Calibration of strength reduction factors to attain target reliability indices of $\beta_T = 3.5$ and $\beta_T = 4.0$ for the proposed xgBoost model.

design is carried out as follows:

i. Provide one layer of externally bonded U-wrapped steel FRCM reinforcement with nominal fiber thickness of 0.084 mm (Table 9) and determine the shear capacity of the beam using the proposed xgBoost model, which is available at: https://github.com/twakjira/FRCM-shear-strengthened-beam. Based on this design, the predicted nominal shear capacity of the beam is 206 kN. Considering the resistance reduction factor of 0.91 calibrated to achieve a reliability level of 3.5 as in ACI 318 [87], the factored resistance (V_r) $= \phi V_n = 0.91 \times \quad 197\text{kN} = 179\text{kN}$, which is less than the applied factored load (200 kN).

Table 9
Design example for FRCM-strengthened beam.

Internal reinforcement				FRCM properties						Resistance	
ρ_{sx}(%)	$f_{sx}(MPa)$	ρ_{sy}(%)	$f_{sy}(MPa)$	Fabric type	Wrapping scheme	t_f (mm)	n_f	ρ_f(‰)	$h_{fe}(mm)$	V_n (kN)	ϕV_n (kN)
3.17	550	0.34	350	Steel	UW	0.084	1	0.933	297	197	179
3.17	550	0.34	350	Steel	UW	0.084	2	1.867	297	248	225
3.17	550	0.34	350	Steel	UW	0.169	2	3.756	297	290	263

ii. Increase the FRCM reinforcement: by increasing the FRCM fabric layers to two, the nominal shear capacity of the beam is increased to 248 kN, as listed in Table 9. Thus, $V_r = \phi V_n = 0.91 \times \quad 248kN = 225kN > V_Q$, which implies that the provided strengthening system is adequate to resist the applied shear.
iii. Check for ductile failure: using section analysis the flexural capacity of the beam is determined to be 256 kN.mm, which corresponds to a load capacity of 256 kN.
iv. Comparing the results in steps (ii) and (iii), it can be observed that the flexural capacity is larger than the shear leading to shear failure, which is not ductile; hence, increase the FRCM reinforcement by increasing the nominal thickness of the fabric. Using two layers of steel fabrics with a nominal thickness of 0.169 mm, the nominal shear capacity is increased to 290 kN (Table 9), which corresponds to $V_r = \phi V_n = 0.91 \times \quad 290kN = 263kN$, which is greater than the load capacity for flexural failure (256 kN).

Therefore, use two layers of steel FRCM fabrics with a nominal thickness of 0.169 mm, tensile strength of 3000 MPa, and elastic modulus of 190 GPa. The designed steel fabric is known by its commercial name as GeoSteel G1200 [90] (Fig. 11).

9. Conclusions

Despite several experimental studies aimed to understand the structural response of RC beams strengthened with FRCM as inorganic composites, there are limited analytical or numerical studies, particularly for shear strengthened RC beams. To this end, data-driven ML-based models to predict the shear capacity of RC beams strengthened with inorganic composites are presented in this paper for the first time. Six ML algorithms; namely, support vector machine, classification and decision trees, random forest, extremely randomized trees, gradient tree boosting, and extreme gradient boosting are evaluated to predict the shear capacity of FRCM shear strengthened RC beams. The developed ML models account for several input parameters that characterize the beam geometry, concrete strength, internal shear and flexural reinforcements, and FRCM system. The following conclusions can be drawn from this study:

- The developed ML-based models are shown to be effective in predicting the shear capacity of FRCM-strengthened RC beams. Among the ML models, xgBoost is the most efficient algorithm in predicting the shear capacity of FRCM-strengthened RC beams with stable and accurate predictions. The experimental shear capacity and predicted values based on the xgBoost model showed the least margins of error and strongest correlation with a coefficient of determination (R^2) of 0.995 and 0.984, for the training and test datasets, respectively.
- Among the existing models, Model-5, which is based on the modified compression field theory resulted in the highest predictive accuracy. The comparisons of the proposed models with the existing formulae confirmed the superiority of the xgBoost model over other models. Moreover, the proposed xgBoost model resulted in the most stable, accurate, and safe predictions. The average of the predicted to experimental shear capacity based on the xgBoost model was 0.99 (STD = 0.06) compared to the mean values of 1.28 (STD = 0.81), 0.66 (STD = 0.26), 0.53 (STD = 0.25), 0.49 (STD = 0.21), 0.94 (STD = 0.22), and 0.90 (STD = 0.28) for the existing models.
- In addition, the proposed xgBoost model substantially reduced the MAE and RMSE compared to the existing models. For instance, the RSME for Model-1, -2, -3, -4, -5, and -6 were 87.02 kN, 81.60 kN, 97.17 kN, 97.21 kN, 37.84 kN, and 50.29 kN respectively. The corresponding value for the proposed xgBoost model was 7.80 kN, which represents 91%, 90%, 92%, 92%, 79%, and 85% reduction in the RMSE relative to Model-1, -2, -3, -4, -5, and -6, respectively.
- Furthermore, the safety, accuracy, and economical aspects of the predictions provided by the proposed and existing models were compared using the Modified Demerits Point Classification method. The proposed xgBoost model provided safe and accurate predictions compared to all other models. Model-1 highly overpredicted the shear capacity of the strengthened beams with more scatter, while Model-4 highly underpredicted the shear capacity of the strengthened beams. The predictions provided by the proposed xgBoost model lie in the appropriate safety region for 98% of the beams compared to only 22%, 18%, 16%, 3%, 51%, and 34% of the beams for Model-1, -2, -3, -4, -5, and -6, respectively.
- The findings of this study showed the successful implementation of machine learning techniques to predict the shear capacity of FRCM-strengthened shear-critical RC beams.

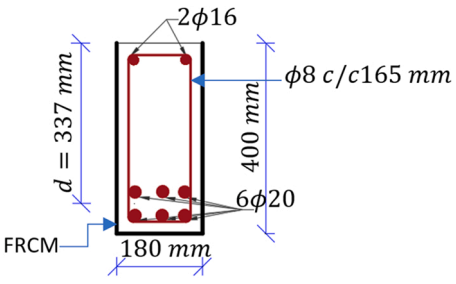

Fig. 11. FRCM-strengthened beam section.

- Finally, the reliability analysis was performed to calibrate the resistance reduction factors that meet two different levels of target reliability indices ($\beta_T = 3.5$ and 4.0) for shear capacity prediction of FRCM-strengthened beams using the proposed xgBoost model. Based on the results of the analysis, resistance reduction factors of 0.91 and 0.87 are calibrated to achieve target reliability levels of 3.5 and 4.0, respectively. A design example is provided using $\phi = 0.91$ for $\beta_T = 3.5$.

The results of this study showed that the existing empirical model and guideline equations are generally not capable of accurately predicting the shear capacity of FRCM-strengthened RC beams, and thus should be modified to account for all the key design parameters that influence the shear capacity of the strengthened beams.

Declaration of Competing Interest

The authors declare that they have no known competing financial interests or personal relationships that could have appeared to influence the work reported in this paper.

Data Availability Statement

Some or all data, models, or code that support the findings of this study are available from the corresponding author upon reasonable request.

Acknowledgment

This paper was made possible by NPRP Grant # NPRP 13S-0209-200311 from the Qatar National Research Fund (a member of Qatar Foundation) and financial support of the Natural Sciences and Engineering Research Council (NSERC) of Canada. Open Access funding provided by the Qatar National Library. The findings achieved herein are solely the responsibility of the authors.

Conflict of Interest

The authors declare that they have no conflict of interest.

References

[1] H. Elsanadedy, H. Abbas, T. Almusallam, Y. Al-Salloum, Organic versus inorganic matrix composites for bond-critical strengthening applications of RC structures – state-of-the-art review, Compos. Part B Eng. (2019) 174, https://doi.org/10.1016/j.compositesb.2019.106947.
[2] T. Triantafillou, C. Papanicolaou, Shear strengthening of reinforced concrete members with textile reinforced mortar (TRM) jackets, Mater. Struct. 39 (2006) 93–103, https://doi.org/10.1617/s11527-005-9034-3.
[3] H. Elsanadedy, T. Almusallam, S. Alsayed, Y. Al-Salloum, Flexural strengthening of RC beams using textile reinforced mortar – experimental and numerical study, Compos. Struct. 97 (2013) 40–55, https://doi.org/10.1016/j.compstruct.2012.09.053.
[4] L. Sneed, S. Verre, C. Carloni, L. Ombres, Flexural behavior of RC beams strengthened with steel-FRCM composite, Eng. Struct. 127 (2016) 686–699, https://doi.org/10.1016/j.engstruct.2016.09.006.
[5] L. Koutas, D. Bournas, Flexural strengthening of two-way RC slabs with textile-reinforced mortar: experimental investigation and design equations, J. Compos. Constr. 21 (2017) 1–11, https://doi.org/10.1061/(ASCE)CC.1943-5614.0000713.
[6] S. Babaeidarabad, G. Loreto, A. Nanni, Flexural strengthening of RC beams with an externally bonded fabric-reinforced cementitious matrix, J. Compos. Constr. 18 (2014) 1–12, https://doi.org/10.1061/(ASCE)CC.1943-5614.0000473.
[7] D. Bournas, P.V. Lontou, C. Papanicolaou, T. Triantafillou, Textile-reinforced mortar versus fiber-reinforced polymer confinement in reinforced concrete columns, ACI Struct. J. 104 (2007) 740–748, https://doi.org/10.14359/18956.
[8] L. Ombres, S. Verre, Structural behaviour of fabric reinforced cementitious matrix (FRCM) strengthened concrete columns under eccentric loading, Compos. Part B Eng. 75 (2015) 235–249, https://doi.org/10.1016/j.compositesb.2015.01.042.
[9] A. Cascardi, F. Longo, F. Micelli, M.A. Aiello, Compressive strength of confined column with Fiber Reinforced Mortar (FRM): new design-oriented-models, Constr. Build. Mater. 156 (2017) 387–401, https://doi.org/10.1016/j.conbuildmat.2017.09.004.
[10] L. Ombres, Concrete confinement with a cement based high strength composite material, Compos. Struct. 109 (2014) 294–304, https://doi.org/10.1016/j.compstruct.2013.10.037.
[11] F. Faleschini, J. Gonzalez-Libreros, M.A. Zanini, L. Hofer, L. Sneed, C. Pellegrino, Repair of severely-damaged RC exterior beam-column joints with FRP and FRCM composites, Compos. Struct. 207 (2019) 352–363, https://doi.org/10.1016/j.compstruct.2018.09.059.
[12] T. Blanksvärd, B. Täljsten, A. Carolin, Shear strengthening of concrete structures with the use of mineral-based composites, J. Compos. Constr. 13 (2009) 25–34, https://doi.org/10.1061/(ASCE)1090-0268(2009)13:1(25).
[13] R. Azam, K. Soudki, J. West, M. Noël, Strengthening of shear-critical RC beams: alternatives to externally bonded CFRP sheets, Constr. Build. Mater. 151 (2017) 494–503, https://doi.org/10.1016/j.conbuildmat.2017.06.106.
[14] Z.C. Tetta, L. Koutas, D. Bournas, Shear strengthening of concrete members with TRM jackets: effect of shear span-to-depth ratio, material and amount of external reinforcement, Compos. Part B Eng. 137 (2018) 184–201, https://doi.org/10.1016/j.compositesb.2017.10.041.
[15] A. Brückner, R. Ortlepp, M. Curbach, Anchoring of shear strengthening for T-beams made of textile reinforced concrete (TRC), Mater. Struct. 41 (2008) 407–418, https://doi.org/10.1617/s11527-007-9254-9.
[16] G. Loreto, S. Babaeidarabad, L. Leardini, A. Nanni, RC beams shear-strengthened with fabric-reinforced-cementitious-matrix (FRCM) composite, Int. J. Adv. Struct. Eng. 7 (2015) 341–352, https://doi.org/10.1007/s40091-015-0102-9.
[17] R. Contamine, A. Si Larbi, P. Hamelin, Identifying the contributing mechanisms of textile reinforced concrete (TRC) in the case of shear repairing damaged and reinforced concrete beams, Eng. Struct. 46 (2013) 447–458, https://doi.org/10.1016/j.engstruct.2012.07.024.
[18] E. Tzoura, T.C. Triantafillou, Shear strengthening of reinforced concrete T-beams under cyclic loading with TRM or FRP jackets, Mater. Struct. 49 (2016) 17–28, https://doi.org/10.1617/s11527-014-0470-9.
[19] K. Jung, K. Hong, S. Han, J. Park, J. Kim, Shear strengthening performance of hybrid FRP-FRCM, Adv. Mater. Sci. Eng. (2015) 2015, https://doi.org/10.1155/2015/564876.

[20] J.H. Gonzalez-Libreros, L.H. Sneed, T. D'Antino, C. Pellegrino, Behavior of RC beams strengthened in shear with FRP and FRCM composites, Eng. Struct. 150 (2017) 830–842, https://doi.org/10.1016/j.engstruct.2017.07.084.
[21] J.H. Gonzalez-Libreros, C. Sabau, L. Sneed, C. Pellegrino, G. Sas, State of research on shear strengthening of RC beams with FRCM composites, Constr. Build. Mater. 149 (2017) 444–458, https://doi.org/10.1016/j.conbuildmat.2017.05.128.
[22] Y. Al-Salloum, H. Elsanadedy, S. Alsayed, R. Iqbal, Experimental and numerical study for the shear strengthening of reinforced concrete beams using textile-reinforced mortar, J. Compos. Constr. 16 (2012) 74–90, https://doi.org/10.1061/(ASCE)CC.1943-5614.0000239.
[23] R. Azam, K. Soudki, FRCM strengthening of shear-critical RC beams, J. Compos. Constr. 18 (2014) 1–9, https://doi.org/10.1061/(ASCE)CC.1943-5614.0000464.
[24] Z.C. Tetta, L. Koutas, D. Bournas, Textile-reinforced mortar (TRM) versus fiber-reinforced polymers (FRP) in shear strengthening of concrete beams, Compos. Part B Eng. 77 (2015) 338–348, https://doi.org/10.1016/j.compositesb.2015.03.055.
[25] C. Escrig, L. Gil, E. Bernat-Maso, F. Puigvert, Experimental and analytical study of reinforced concrete beams shear strengthened with different types of textile-reinforced mortar, Constr. Build. Mater. 83 (2015) 248–260, https://doi.org/10.1016/j.conbuildmat.2015.03.013.
[26] O. Awani, T. El Maaddawy, A. Refai, Numerical simulation and experimental testing of concrete beams strengthened in shear with fabric-reinforced cementitious matrix, J. Compos. Constr. 20 (2015) 04016056, https://doi.org/10.1061/(ASCE)CC.1943-5614.0000711.
[27] L. Ombres, Structural performances of reinforced concrete beams strengthened in shear with a cement based fiber composite material, Compos. Struct. 122 (2015) 316–329, https://doi.org/10.1016/j.compstruct.2014.11.059.
[28] Z.C. Tetta, L. Koutas, D. Bournas, Shear strengthening of full-scale RC T-beams using textile-reinforced mortar and textile-based anchors, Compos. Part B Eng. 95 (2016) 225–239, https://doi.org/10.1016/j.compositesb.2016.03.076.
[29] A. Brückner, R. Ortlepp, M. Curbach, Textile reinforced concrete for strengthening in bending and shear, Mater. Struct. 39 (2006) 741–748, https://doi.org/10.1617/s11527-005-9027-2.
[30] T.G. Wakjira, U. Ebead, FRCM/internal transverse shear reinforcement interaction in shear strengthened RC beams, Compos. Struct. 201 (2018) 326–339, https://doi.org/10.1016/j.compstruct.2018.06.034.
[31] A. Younis, U. Ebead, K. Shrestha, Different FRCM systems for shear-strengthening of reinforced concrete beams, Constr. Build. Mater. 153 (2017) 514–526, https://doi.org/10.1016/j.conbuildmat.2017.07.132.
[32] A. Si Larbi, R. Contamine, E. Ferrier, P. Hamelin, Shear strengthening of RC beams with textile reinforced concrete (TRC) plate, Constr. Build. Mater. 24 (2010) 1928–1936, https://doi.org/10.1016/j.conbuildmat.2010.04.008.
[33] ACI Committee 549, Guide to Design and Construction of Externally Bonded Fabric- Reinforced Cementitious Matrix (FRCM) Systems for Repair and Strengthening Concrete and Masonry Structures (ACI 549.4R-13), American Concrete Institute, Farmington Hills, MI, USA, 2013.
[34] T.G. Wakjira, U. Ebead, A shear design model for RC beams strengthened with fabric reinforced cementitious matrix, Eng. Struct. 200 (2019), 109698, https://doi.org/10.1016/j.engstruct.2019.109698.
[35] T.G. Wakjira, U. Ebead, Simplified compression field theory-based model for shear strength of fabric-reinforced cementitious matrix- strengthened reinforced concrete beams, ACI Struct. J. 117 (2020) 91–104, https://doi.org/10.14359/51721366.
[36] T.G. Wakjira, U. Ebead, Internal transverse reinforcement configuration effect of EB/NSE-FRCM shear strengthening of RC deep beams, Compos. Part B Eng. 166 (2019) 758–772, https://doi.org/10.1016/j.compositesb.2019.03.004.
[37] U. Ebead, T.G. Wakjira, FRCM/stirrups interaction in RC beams strengthened in shear using NSE-FRCM, IOP Conf. Ser. Mater. Sci. Eng. 431 (2018), 112001, https://doi.org/10.1088/1757-899X/431/11/112001.
[38] I. Flood, Towards the next generation of artificial neural networks for civil engineering, Adv. Eng. Inform. 22 (2008) 4–14, https://doi.org/10.1016/j.aei.2007.07.001.
[39] W. Yan, L. Deng, F. Zhang, T. Li, S. Li, Probabilistic machine learning approach to bridge fatigue failure analysis due to vehicular overloading, Eng. Struct. 193 (2019) 91–99, https://doi.org/10.1016/j.engstruct.2019.05.028.
[40] J.C. Weinstein, M. Sanayei, M. Asce, B.R. Brenner, F. Asce, Bridge damage identification using artificial neural networks, J. Bridge Eng. 23 (2018) 04018084, https://doi.org/10.1061/(ASCE)BE.1943-5592.0001302.
[41] E. Fathalla, Y. Tanaka, K. Maekawa, Remaining fatigue life assessment of in-service road bridge decks based upon arti fi cial neural networks, Eng. Struct. 171 (2018) 602–616, https://doi.org/10.1016/j.engstruct.2018.05.122.
[42] S. Mangalathu, S.H. Hwang, E. Choi, J.S. Jeon, Rapid seismic damage evaluation of bridge portfolios using machine learning techniques, Eng. Struct. (2019) 201, https://doi.org/10.1016/j.engstruct.2019.109785.
[43] K. Morfidis, K. Kostinakis, Approaches to the rapid seismic damage prediction of r/c buildings using artificial neural networks, Eng. Struct. 165 (2018) 120–141, https://doi.org/10.1016/j.engstruct.2018.03.028.
[44] H. Naderpour, A. Kheyroddin, G.G. Amiri, Prediction of FRP-confined compressive strength of concrete using artificial neural networks, Compos. Struct. 92 (2010) 2817–2829, https://doi.org/10.1016/j.compstruct.2010.04.008.
[45] D. Feng, Z.T. Liu, X.D. Wang, Y. Chen, J.Q. Chang, D.F. Wei, et al., Machine learning-based compressive strength prediction for concrete: an adaptive boosting approach, Constr. Build. Mater. (2020) 230, https://doi.org/10.1016/j.conbuildmat.2019.117000.
[46] W. Ben Chaabene, M. Flah, M. Nehdi, Machine learning prediction of mechanical properties of concrete: critical review, Constr. Build. Mater. 260 (2020), 119889, https://doi.org/10.1016/j.conbuildmat.2020.119889.
[47] Y. Yu, W. Li, J. Li, T.N. Nguyen, A novel optimised self-learning method for compressive strength prediction of high performance concrete, Constr. Build. Mater. 184 (2018) 229–247, https://doi.org/10.1016/j.conbuildmat.2018.06.219.
[48] D. Feng, W.J. Wang, S. Mangalathu, G. Hu, T. Wu, Implementing ensemble learning methods to predict the shear strength of RC deep beams with/without web reinforcements, Eng. Struct. (2021) 235, https://doi.org/10.1016/j.engstruct.2021.111979.
[49] D. Feng, Z.T. Liu, X.D. Wang, Z.M. Jiang, S.X. Liang, Failure mode classification and bearing capacity prediction for reinforced concrete columns based on ensemble machine learning algorithm, Adv. Eng. Inform. (2020) 45, https://doi.org/10.1016/j.aei.2020.101126.
[50] S.M. Reza, M.S. Alam, S. Tesfamariam, Lateral load resistance of bridge piers under flexure and shear using factorial analysis, Eng. Struct. 59 (2014) 821–835, https://doi.org/10.1016/j.engstruct.2013.12.009.
[51] R. Perera, D. Tarazona, A. Ruiz, A. Martín, Application of artificial intelligence techniques to predict the performance of RC beams shear strengthened with NSM FRP rods. Formulation of design equations, Compos. Part B Eng. 66 (2014) 162–173, https://doi.org/10.1016/j.compositesb.2014.05.001.
[52] S. Mangalathu, J.-S. Jeon, Machine learning–based failure mode recognition of circular reinforced concrete bridge columns: comparative study, J. Struct. Eng. 145 (2019) 04019104, https://doi.org/10.1061/(asce)st.1943-541x.0002402.
[53] S. Mangalathu, J. Jeon, Classification of failure mode and prediction of shear strength for reinforced concrete beam-column joints using machine learning techniques, Eng. Struct. 160 (2018) 85–94, https://doi.org/10.1016/j.engstruct.2018.01.008.
[54] D.-C. Feng, W.-J. Wang, S. Mangalathu, E. Taciroglu, Interpretable XGBoost-SHAP machine-learning model for shear strength prediction of squat RC walls, J. Struct. Eng. 147 (2021) 04021173, https://doi.org/10.1061/(ASCE)ST.1943-541X.0003115.
[55] B. Fu, D. Feng, A machine learning-based time-dependent shear strength model for corroded reinforced concrete beams, J. Build. Eng. (2021) 36, https://doi.org/10.1016/j.jobe.2020.102118.
[56] B. Keshtegar, M.L. Nehdi, N.T. Trung, R. Kolahchi, Predicting load capacity of shear walls using SVR–RSM model [Formula presented], Appl. Soft Comput. (2021) 112, https://doi.org/10.1016/j.asoc.2021.107739.
[57] M.K. Almustafa, M.L. Nehdi, Machine learning prediction of structural response for FRP retrofitted RC slabs subjected to blast loading, Eng. Struct. 244 (2021), 112752, https://doi.org/10.1016/j.engstruct.2021.112752.
[58] S. Mangalathu, S. Hwang, J. Jeon, Failure mode and effects analysis of RC members based on machine-learning-based SHapley Additive exPlanations (SHAP) approach, Eng. Struct. 219 (2020), 110927, https://doi.org/10.1016/j.engstruct.2020.110927.

[59] H. Salehi, R. Burgueño, Emerging artificial intelligence methods in structural engineering, Eng. Struct. 171 (2018) 170–189, https://doi.org/10.1016/j.engstruct.2018.05.084.
[60] R. Bashir, A. Ashour, Neural network modelling for shear strength of concrete members reinforced with FRP bars, Compos. Part B Eng. 43 (2012) 3198–3207, https://doi.org/10.1016/j.compositesb.2012.04.011.
[61] S. Lee, C. Lee, Prediction of shear strength of FRP-reinforced concrete flexural members without stirrups using artificial neural networks, Eng. Struct. 61 (2014) 99–112, https://doi.org/10.1016/j.engstruct.2014.01.001.
[62] R. Perera, M. Barchín, A. Arteaga, A.De Diego, Prediction of the ultimate strength of reinforced concrete beams FRP-strengthened in shear using neural networks, Compos. Part B Eng. 41 (2010) 287–298, https://doi.org/10.1016/j.compositesb.2010.03.003.
[63] H.M. Tanarslan, M. Secer, A. Kumanlioglu, An approach for estimating the capacity of RC beams strengthened in shear with FRP reinforcements using artificial neural networks, Constr. Build. Mater. 30 (2012) 556–568, https://doi.org/10.1016/j.conbuildmat.2011.12.008.
[64] L. Breiman, J.H. Friedman, R. Olshen, C. Stone, Classification and Regression Trees, Wadsworth, Belmont, CA, 1984.
[65] K. Yan, C. Shi, Prediction of elastic modulus of normal and high strength concrete by support vector machine, Constr. Build. Mater. 24 (2010) 1479–1485, https://doi.org/10.1016/j.conbuildmat.2010.01.006.
[66] S. Mangalathu, H. Shin, E. Choi, J.S. Jeon, Explainable machine learning models for punching shear strength estimation of flat slabs without transverse reinforcement, J. Build. Eng. 39 (2021), 102300, https://doi.org/10.1016/j.jobe.2021.102300.
[67] J. Rahman, K.S. Ahmed, N.I. Khan, K. Islam, S. Mangalathu, Data-driven shear strength prediction of steel fiber reinforced concrete beams using machine learning approach, Eng. Struct. (2021) 233, https://doi.org/10.1016/j.engstruct.2020.111743.
[68] H.D. Nguyen, G.T. Truong, M. Shin, Development of extreme gradient boosting model for prediction of punching shear resistance of r/c interior slabs, Eng. Struct. (2021) 235, https://doi.org/10.1016/j.engstruct.2021.112067.
[69] S. Mangalathu, H. Jang, S.-H. Hwang, J.-S. Jeon, Data-driven machine-learning-based seismic failure mode identification of reinforced concrete shear walls, Eng. Struct. 208 (2020), 110331, https://doi.org/10.1016/j.engstruct.2020.110331.
[70] T.G. Wakjira, M.S. Alam, U. Ebead, Plastic hinge length of rectangular RC columns using ensemble machine learning model, Eng. Struct. 244 (2021), 112808, https://doi.org/10.1016/j.engstruct.2021.112808.
[71] T.G. Wakjira, A. Al-Hamrani, U. Ebead, W. Alnahhal, Shear capacity prediction of FRP-RC beams using single and ensenble ExPlainable Machine learning models, Compos. Struct. 287 (2022), 115381, https://doi.org/10.1016/j.compstruct.2022.115381.
[72] E.C. Bentz, F.J. Vecchio, M.P. Collins, Simplified compression field theory for calculating shear strength of reinforced concrete elements, ACI Struct. J. 103 (2006) 614–624, https://doi.org/10.14359/16438.
[73] D. Marcinczak, T. Trapko, Shear strengthening of reinforced concrete beams with PBO-FRCM composites with anchorage, Compos. Part B Eng. 158 (2019) 149–161, https://doi.org/10.1016/j.compositesb.2018.09.061.
[74] G.E. Thermou, V.K. Papanikolaou, C. Lioupis, I. Hajirasouliha, Steel-reinforced grout (SRG) strengthening of shear-critical RC beams, Constr. Build. Mater. 216 (2019) 68–83, https://doi.org/10.1016/j.conbuildmat.2019.04.259.
[75] T.G. Wakjira, U. Ebead, Experimental and analytical study on strengthening of reinforced concrete T-beams in shear using steel reinforced grout (SRG), Compos. Part B Eng. 177 (2019), 107368, https://doi.org/10.1016/j.compositesb.2019.107368.
[76] T.G. Wakjira, U. Ebead, Shear span-to-depth ratio effect on steel reinforced grout strengthened reinforced concrete beams, Eng. Struct. 216 (2020), 110737, https://doi.org/10.1016/j.engstruct.2020.110737.
[77] T.G. Wakjira, U. Ebead, Strengthening of reinforced concrete beams in shear using different steel reinforced grout techniques, Struct. Concr. (2020), https://doi.org/10.1002/suco.202000354.
[78] C. Cortes, V. Vapnik, Support-vector networks, Mach. Learn. 20 (1995) 273–297, https://doi.org/10.1109/64.163674.
[79] S. Theodoridis, Learning in Reproducing Kernel Hilbert Spaces, 2015. ⟨https://doi.org/10.1016/b978-0-12-801522-3.00011-2⟩.
[80] T.M. Mitchell, Machine Learning and Data Mining, vol. 42, 1999. ⟨https://doi.org/10.1145/319382.319388⟩.
[81] V. Cherkassky, Y. Ma, Practical selection of SVM parameters and noise estimation for SVM regression, Neural Netw. 17 (2004) 113–126, https://doi.org/10.1016/S0893-6080(03)00169-2.
[82] L. Breiman, Random forests, Mach. Learn. 45 (2001) 5–32.
[83] P. Geurts, D. Ernst, L. Wehenkel, Extremely randomized trees, Mach. Learn. 63 (2006) 3–42, https://doi.org/10.1007/s10994-006-6226-1.
[84] J.H. Friedman, Greedy function approximation: a gradient boosting machine, Ann. Stat. (2001) 1189–1232, https://doi.org/10.1214/aos/1013203451.
[85] T. Chen, C. Guestrin, Xgboost: a scalable tree boosting system, in: Proceedings of the 22nd SIGKDD Conference on Knowledge Discovery and Data Mining, 2016.
[86] B.N.M. Neto, J.A.O. Barros, G.S.S.A. Melo, Model to simulate the contribution of fiber reinforcement for the punching resistance of RC slabs, J. Mater. Civ. Eng. 26 (2014) 04014020, https://doi.org/10.1061/(ASCE)MT.1943-5533.
[87] American Concrete Institute ACI Committee 318, Building code requirements for structural concrete (ACI 318-14): an ACI standard: commentary on building code requirements for structural concrete (ACI 318R-14), an ACI report, 2014.
[88] M.M. Szerszen, A.S. Nowak, Calibration of design code for buildings (ACI 318): Part 2 – reliability analysis and resistance factors, ACI Struct. J. 100 (2003) 383–391, https://doi.org/10.14359/12614.
[89] J.K. Wight. Reinforced Concrete Mechanics and Design, 7th edition, Pearson Education Inc, Hoboken, New Jersey, 2016.
[90] Kerakoll - The GreenBuilding Company , n.d., ⟨www.kerakoll.com⟩, (Accessed 25 December 2018).